Int. J. Electrochem. Sci., 8 **(2013)** 11526 - 11545

International Journal of ELECTROCHEMICAL SCIENCE
www.electrochemsci.org

Electrochemical and Gravimetric Evaluation of 7-methyl-2-phenylimidazo[1,2-α]pyridine of Carbon Steel Corrosion in Phosphoric Acid Solution

D. Ben Hmamou[1], *R. Salghi*[1], *A. Zarrouk*[2,*], *H. Zarrok*[3], *B. Hammouti*[2], *S. S. Al-Deyab*[4], *A. El Assyry*[6], *N. Benchat*[2], *M. Bouachrine*[5]

[1] Laboratory of Environmental Engineering and Biotechnology, ENSA, University Ibn Zohr, PO Box 1136, 80000 Agadir, Morocco.
[2] LCAE-URAC 18, Faculty of Science, University of Mohammed Premier, Po Box 717 60000 Oujda, Morocco.
[3] Laboratory separation processes, Faculty of Science, University Ibn Tofail PO Box 242, Kenitra, Morocco.
[4] Petrochemical Research Chair, Chemistry Department, College of Science, King Saud University, P.O. Box 2455, Riyadh 11451, Saudi Arabia.
[5] ESTM, Université Moualy Ismail, Meknes, Morocco.
[6] Laboratoire d'Optoélectronique et de Physico-chimie des Matériaux (Unité associée au CNRST), Université Ibn Tofail, Département de Physique, B.P. 133, Kénitra, Maroc
[*]E-mail: azarrouk@gmail.com

Received: 4 March 2013 / *Accepted:* 1 August 2013 / *Published:* 20 August 2013

The inhibition effect of 7-methyl-2-phenylimidazo[1,2-α]pyridine (PIP) on the corrosion of carbon steel in phosphoric acid solution was investigated for the first time by weight loss, potentiodynamic polarization, electrochemical impedance spectroscopy (EIS) and quantum chemicals calculations. It was observed that inhibition efficiency increased with increasing inhibitor concentration. Potentiodynamic polarization studies show that PIP acts as a mixed type inhibitor. AC impedance results were interpreted using an equivalent circuit in which a constant phase element (CPE) was used in place of a double layer capacitance (C_{dl}) in order to give more accurate fit to the experimental results. The kinetic data such as apparent activation energies and pre-exponential factors at optimum concentration of the inhibitor were calculated and discussed. Adsorption of PIP molecules on carbon steel surface was found to obey the Langmuir adsorption isotherm. The relations between quantum chemical parameters and corrosion inhibition efficiency have been discussed to see if there is any correlation between the two of them.

Keywords: Pyridine derivative, Steel, Corrosion inhibition, Polarization curves, EIS, DFT

1. INTRODUCTION

Acid solutions are widely used in many industrial processes. Besides hydrochloric acid, phosphoric acid and sulfuric acid are regular aggressive solutions for acid picking, acid cleaning and acid descaling due to their special chemical properties. The use of corrosion inhibitor is one of the most practical methods for protecting the corrosion of metal. As a result, corrosion inhibitors for hydrochloric acid, phosphoric acid and sulfuric acid have attracted increasing attention due to their extended applications [1-26].

Corrosion inhibitors can be used to prevent metal from corrosion in corrosive media. Generally the studies on corrosion inhibitors are mainly focusing on three domains: one is to find appropriate inhibitor among the known compounds, and the next is to synthesize new compounds under the direction of theoretical calculation, and the last is search the synergistic action among various compounds to expand the range of inhibitor application.

Phosphoric acid (H_3PO_4) is widely used in the surface treatment of steel such as chemical and electrolytic polishing, chemical coloring, chemical and electrolytic etching, removal of oxide film, phosphating, passivating, and surface cleaning. However, phosphoric acid shows strong corrosiveness on ferrous and ferrous alloys. Accordingly, there is a great need to protect steel in the phosphoric acid medium. Up to now, little work [27-31] appears to have been done on the inhibition of steel in H_3PO_4 solution.

The objective of this investigation is to determine the corrosion inhibition efficiency of 7-methyl-2-phenylimidazo[1,2-α]pyridine as a novel inhibitor for the corrosion of carbon steel in 2.0 M H_3PO_4 and to calculate the surface parameters of the pyridine derivative. The inhibition efficiency was determined using three different techniques: electrochemical impedance spectroscopy (EIS), potentiodynamic polarization and gravimetric measurements. The chemical structure of the studied pyridine derivative is given in Fig 1.

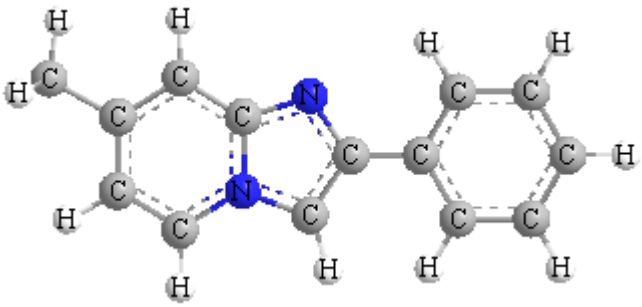

Figure 1. The chemical structure of the studied pyridine compound.

2. EXPERIMENTAL METHODS

2.1. Materials

The steel used in this study is carbon steel (Euronorm: C35E carbon steel and US specification: SAE 1035) with a chemical composition (in wt%) of 0.370 % C, 0.230 % Si, 0.680 %

Mn, 0.016 % S, 0.077 % Cr, 0.011 % Ti, 0.059 % Ni, 0.009 % Co, 0.160 % Cu and the remainder iron (Fe). The carbon steel samples were pre-treated prior to the experiments by grinding with emery paper SiC (120, 600 and 1200); rinsed with distilled water, degreased in acetone in an ultrasonic bath immersion for 5 min, washed again with bidistilled water and then dried at room temperature before use. The acids solution (2.0 M H_3PO_4) was prepared by dilution of an analytical reagent grade 85% H_3PO_4 with double-distilled water. The concentration range of PIP employed was 10^{-6} M to 10^{-3} M.

2.3. Measurements

2.3.1. Weight loss measurements

Gravimetric measurements were carried out at definite time interval of 2 h at room temperature using an analytical balance (precision ± 0.1 mg). The carbon steel specimens used have a rectangular form (length = 1.6 cm, width = 1.6 cm, thickness = 0.07 cm). Gravimetric experiments were carried out in a double glass cell equipped with a thermostated cooling condenser containing 80 mL of non-de-aerated test solution. After immersion period, the steel specimens were withdrawn, carefully rinsed with bidistilled water, ultrasonic cleaning in acetone, dried at room temperature and then weighted. Triplicate experiments were performed in each case and the mean value of the weight loss was calculated.

2.3.2. Electrochemical measurements

Electrochemical experiments were conducted using impedance equipment (Tacussel-Radiometer PGZ 100) and controlled with Tacussel corrosion analysis software model Voltamaster 4. A conventional three-electrode cylindrical Pyrex glass cell was used. The temperature was thermostatically controlled. The working electrode was carbon steel with the surface area of 1 cm^2. A saturated calomel electrode (SCE) was used as a reference. All potentials were given with reference to this electrode. The counter electrode was a platinum plate of surface area of 1 cm^2. A saturated calomel electrode (SCE) was used as the reference; a platinum electrode was used as the counter-electrode. All potentials are reported *vs*. SCE. All electrochemical tests have been performed in aerated solutions at 298 K.

For polarization curves, the working electrode was immersed in a test solution during 30 min until a steady state open circuit potential (E_{ocp}) was obtained. The polarization curve was recorded from -800 to -200 mV/SCE with a scan rate of 1 mV s^{-1}. AC impedance measurements were carried-out in the frequency range of 100 kHz to 10 mHz, with 10 points per decade, at the rest potential, after 30 min of acid immersion, by applying 10 mV ac voltage peak-to-peak. Nyquist plots were made from these experiments. The best semicircle was fit through the data points in the Nyquist plot using a non-linear least square fit so as to give the intersections with the *x*-axis.

2.3. Quantum chemical calculations

All theoretical calculations were performed using DFT (density functional theory) with the Beck's three parameter exchange functional along with the Lee-Yang-Parr nonlocal correlation functional (B3LYP) [32-34] with 6-31G* basis set is implemented in Gaussian 03 program package [35]. This approach is shown to yield favourable geometries for a wide variety of systems. The following quantum chemical parameters were calculated from the obtained optimized molecular structure: the energy of the highest occupied molecular orbital (E_{HOMO}), the energy of the lowest unoccupied molecular orbital (E_{LUMO}), the energy band gap ($\Delta E_{gap} = E_{HOMO} - E_{LUMO}$), the dipole moment ($\mu$), the electron affinity (A), the ionization potential (I) and the number of transferred electrons (ΔN).

3. RESULTS AND DISCUSSION

3.1. Effect of concentration inhibitor

3.1.1. Polarization curves

In order to examine an influence of 7-methyl-2-phenylimidazo[1,2-α]pyridine (PIP) on acidic corrosion of carbon steel the potentiodynamic polarization was performed. Fig. 2 presents Tafel polarization characteristics of carbon steel in 2.0 M H_3PO_4 containing different concentrations of PIP. It can be seen from the plot that anodic current densities decreased after the addition of PIP and corrosion potentials (E_{corr}) were shifted towards the direction of more noble values. Thus it is evident that anodic process was affected depending on the PIP concentration while the same increase in the concentration did not influence significantly the cathodic process. Table 1 demonstrates Tafel parameters such as the cathodic Tafel slope (b_c), corrosion potential (E_{corr}), corrosion current densities (I_{corr}), the percentage inhibition efficiency is symbolized as η_p (%) and calculated using the following Eq. (1):

$$\eta_p(\%) = \left(\frac{i_{corr(uninh)} - i_{corr(inh)}}{i_{corr(uninh)}} \right) \times 100 \qquad (1)$$

where $i_{corr(uninh)}$ and $i_{corr(inh)}$ are uninhibited and inhibited corrosion current densities, respectively.

It is illustrated from the data listed in Table 1, that both anodic metal dissolution of iron and cathodic hydrogen evolution reaction were inhibited after the addition of PIP to 2.0 M H_3PO_4 solution. The inhibition of these reactions was more pronounced on increasing PIP concentration. The lower corrosion current density I_{corr} values in the presence of inhibitor without causing significant changes in corrosion potential ($-488 \leq E_{corr}$ (mV/SCE) ≤ -452) suggests that, the compound is mixed type inhibitor (i.e., inhibits both anodic and cathodic reactions) and is adsorbed on the surface, thereby blocking the corrosion reaction. In presence of PIP, the corrosion potential E_{corr} of carbon steel shifted to the range (4-36) mV/SCE, compared to the blank.

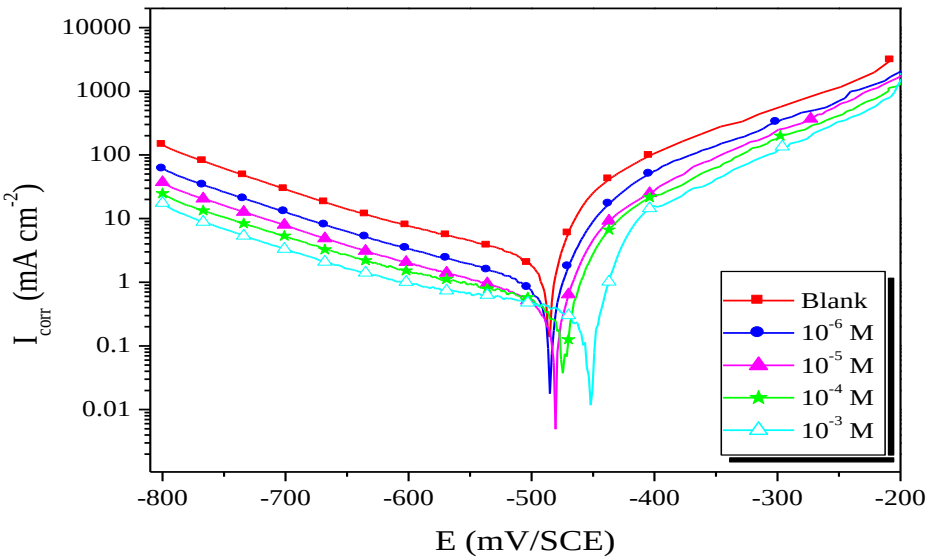

Figure 2. Potentiodynamic polarisation curves of carbon steel in 2.0 M H_3PO_4 in the presence of different concentrations of PIP.

According to Yan et al. [36] an inhibitor can be classified as cathodic or anodic type if the displacement in corrosion potential is more than 85 mV/SCE, with respect to corrosion potential of the blank. This confirms that PIP extract acts as mixed-type inhibitor. The observed decrease of the current densities I_{corr} with the increase in PIP concentration, indicating the increased inhibition efficiency with the increase in the concentration of the inhibitor. This reflects also, the formation of anodic protective films containing oxides and PIP.

Table 1. Electrochemical parameters of carbon steel at various concentrations of PIP in 2.0 M H_3PO_4 and corresponding inhibition efficiency.

Inhibitor	Conc (M)	E_{corr} (mV/SCE)	I_{corr} (μA/cm^2)	$-b_c$ (mV/dec)	η_p (%)
Blank	2.00	-488	2718	135	---
PIP	10^{-3}	-452	241.0	154	91.1
	10^{-4}	-474	463.0	148	83.0
	10^{-5}	-480	775.0	145	78.8
	10^{-6}	-484	1020	150	62.5

3.1.2. Electrochemical impedance spectroscopy measurements

Fig. 3 shows the Nyquist diagrams for synthesized corrosion inhibitor in 2.0 M H_3PO_4 at OCP and 298K without and with various concentrations of the inhibitor. These diagrams have similar shape throughout all tested concentrations, indicating that almost no change in the corrosion mechanism

occurs due to the inhibitor addition [37]. The high frequency loops are not perfect semicircles which can be attributed to the frequency dispersion as a result of the roughness and inhomogeneous of electrode surface [38]. The Nyquist plots (Fig. 3) show a depressed capacitive loop in the high frequency range. The capacitive loop can be attributed to the charge transfer reaction and time constant of the electric double layer and to the surface inhomogeneity of structural or interfacial origin, such as those found in adsorption processes. Furthermore, the diameter of the capacitive loop in the presence of inhibitor is bigger than that in the absence of inhibitor (blank solution) and increases with the inhibitor concentration. This indicated that the impedance of inhibited substrate increased with increasing of the corrosion inhibitor concentration.

It should be noted that the best fit of experimental data to this single time constant model was obtained using a constant phase element (CPE) rather than an ideal capacitor. Electrochemical parameters derived from the electrical model of Fig. 4 are given in Table 2. Inhibition efficiency in Table 2 was calculated according to following equation:

$$\eta_i = \left(\frac{R_{ct(inh)} - R_{ct(uninh)}}{R_{ct(inh)}} \right) \times 100 \qquad (2)$$

where $R_{ct(inh)}$ and $R_{ct(uninh)}$ are the charge-transfer resistance values with and without inhibitor, respectively.

Various parameters such as charge transfer resistance (R_{ct}), solution resistance (R_s), double layer capacitance (C_{dl}) and inhibition efficiency (η_i) were calculated and listed in Table 2. From Table 2, it was revealed that R_{ct} values increases prominently while C_{dl} reduces with increasing of the concentration of synthesized inhibitor. The decrease in C_{dl} compared with that in blank solution (without inhibitor), which can result from a decrease in local dielectric constant and/or an increase in the thickness of the electrical double layer, suggested that the inhibitor species function by adsorption at the metal/solution interface [39]. The inhibition efficiency increased with increasing the corrosion inhibitor concentration and the maximum inhibition efficiency reached up to 92.6%, which further confirms that the synthesized inhibitor exhibits very good inhibitive performance for carbon steel in 2.0 M H_3PO_4.

According to Table 2, as the concentration of pyridine derivative increases, the charge transfer resistance (R_{ct}) increases slightly, indicating formation of an insulated inhibitor layer on metal surface. In Table 2 the double layer capacitance C_{dl} was calculated by Eq. (3):

$$C_{dl} = \frac{\left(Y_0 . R_{ct}\right)^{1/n}}{R_{ct}} \qquad (3)$$

where Y_0 and n are CPE parameters. The parameter "n" of the CPE is an indicator of electrode surface roughness or heterogeneity and parameter "Y_0" is considered to be the CPE admittance. According to Table 2, as the concentration of pyridine derivative increases the double layer capacitance decreases.

The double layer capacitance can also be expressed in the Helmholtz model by Eq. (4):

$$C_{dl} = \frac{\varepsilon_0 . \varepsilon}{\delta} S \qquad (4)$$

where δ is the thickness of electrical double layer, S is the surface of the electrode, ε_0 is the permittivity of vacuum and ε is the medium dielectric constant. The decrease in C_{dl} values may be interpreted either by a decrease of local dielectric constant (ε) or increase of electrical double layer thickness (δ) on the metal surface [40].

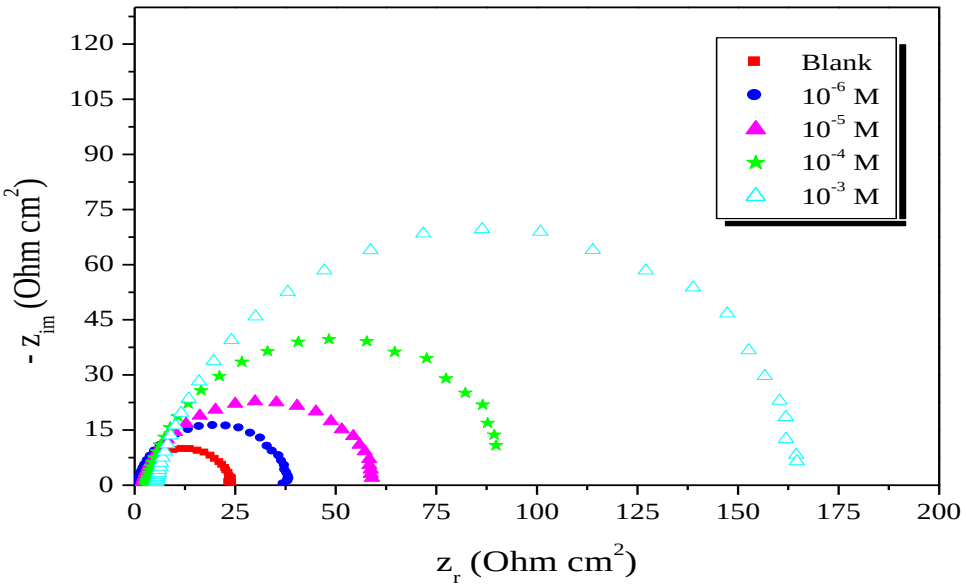

Figure 3. Nyquist diagrams for carbon steel electrode with and without PIP at E_{corr} after 30 min of immersion.

The double layer capacitance decline could be related to the decrease of local dielectric constant (ε) or increase of thickness of electrical double layer due to the adsorption of pyridine derivative on the metal surface.

Solution resistance (R_s) increases after addition of inhibitor which could be attributed to protonation of inhibitors and proton ion (H^+) consumption.

Table 2. Electrochemical Impedance parameters for corrosion of carbon steel in acid medium at various contents of PIP.

	Conc (M)	R_s (Ω cm^2)	R_{ct} (Ω cm^2)	n	Y_0 (s^n/Ω cm^2)	C_{dl} (μF/cm^2)	η_i (%)
Blank	2.0	1.20	14.00	0.88	0.00021024	94.96	----
MPP	10^{-3}	5.42	188.7	0.89	0.000030945	16.38	92.6
	10^{-4}	3.12	94.30	0.88	0.000055433	27.07	85.1
	10^{-5}	1.65	62.04	0.89	0.000080972	42.09	77.43
	10^{-6}	1.41	37.73	0.89	0.000101140	50.81	62.9

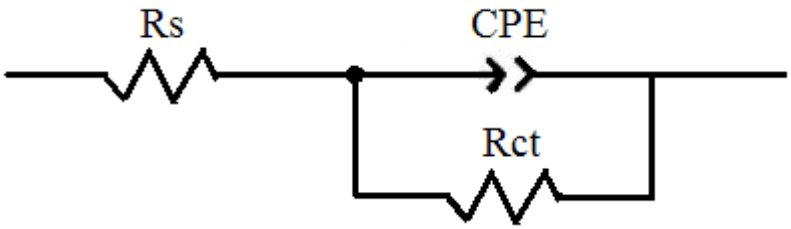

Figure 4. Equivalent electrical circuit corresponding to the corrosion process on the carbon steel in phosphoric acid.

3.1.3. Weight loss

The spontaneous dissolution of carbon steel in 2.0 M H_3PO_4 solutions containing different concentrations of pyridine derivative was studied by weight loss measurements. Fig. 5 shows the variations of corrosion rate calculated from weight loss measurements and corresponding inhibition efficiency at different concentrations of pyridine derivative at 298K. The corrosion rate, degree of surface coverage and inhibition efficiencies can be calculated from equations [41]:

$$A = \frac{\Delta W}{St} \qquad (5)$$

$$\theta = \frac{A_{uninh} - A_{inh}}{A_{uninh}} \qquad (6)$$

$$\eta_w = \left(\frac{A_{uninh} - A_{inh}}{A_{uninh}} \right) \times 100 \qquad (7)$$

where ΔW is the average weight loss (mg), S is the surface area of specimens (cm^2), and t is the immersion time (h), A_{uninh} and A_{inh} are corrosion rates in the absence and presence of inhibitor, respectively.

Table 3. Regroups the results of weight loss of carbon steel in 2.0 M H_3PO_4 with and without the addition of various concentrations of the PIP.

Inhibitor	Conc (M)	A (mg cm^{-2} h^{-1})	η_w (%)	θ
Blank	2.0	1.972	----	----
PIP	10^{-3}	0.118	94.0	0.940
	10^{-4}	0.271	86.2	0.862
	10^{-5}	0.530	73.1	0.731
	10^{-6}	0.821	58.4	0.584

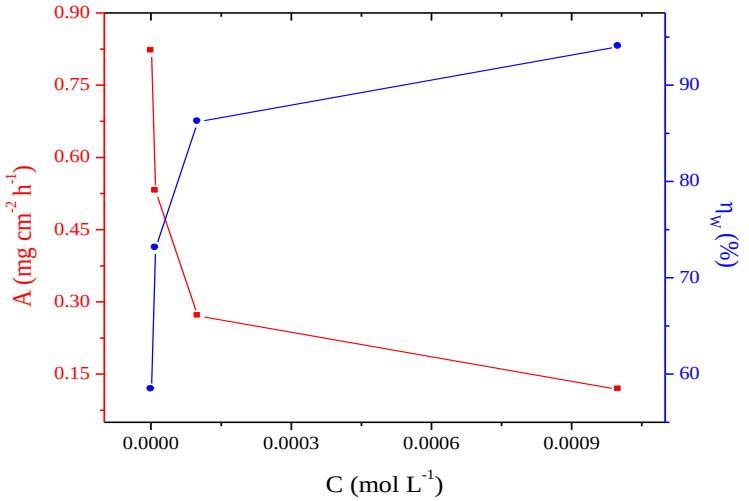

Figure 5. Variations of the corrosion rate calculated from weight loss measurements and corresponding inhibition efficiency at different concentrations of PIP in 2.0 M H_3PO_4 solutions.

The corrosion parameters such as inhibition efficiency (η_W%) and corrosion rate (A) at different concentration of PIP in 2.0 M H_3PO_4 at 298K are presented in Table 3. As can be seen from Table 3, pyridine derivative inhibits the corrosion of carbon steel at all concentrations. Data in Table 3 reveal that the inhibition efficiency increases with increasing concentration of PIP. The corrosion inhibition can be attributed to the adsorption of PIP molecules at steel/ H_3PO_4 solution interface [42].

3.2. Effect of temperature and Corrosion kinetic parameters

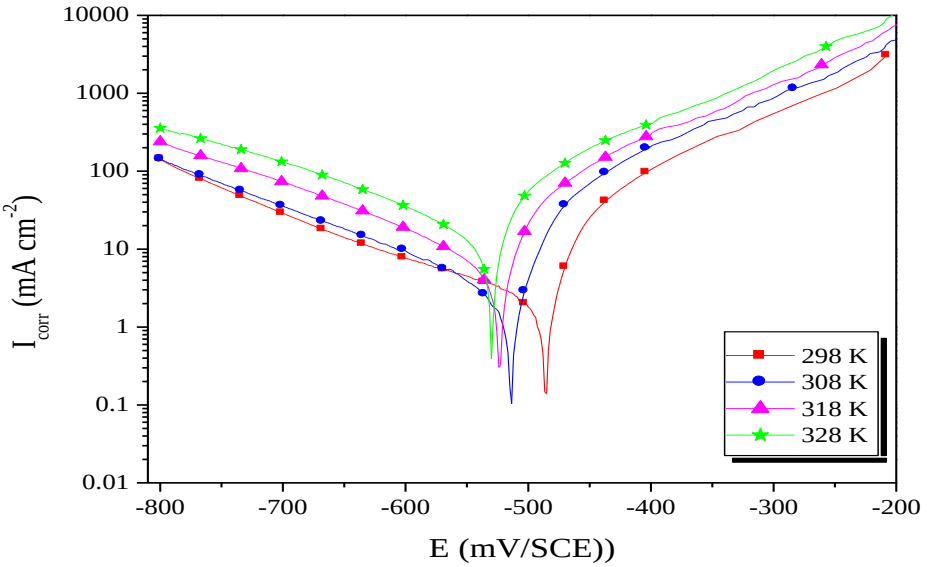

Figure 6. Potentiodynamic polarisation curves of carbon steel in 2.0 M H_3PO_4 at different temperatures.

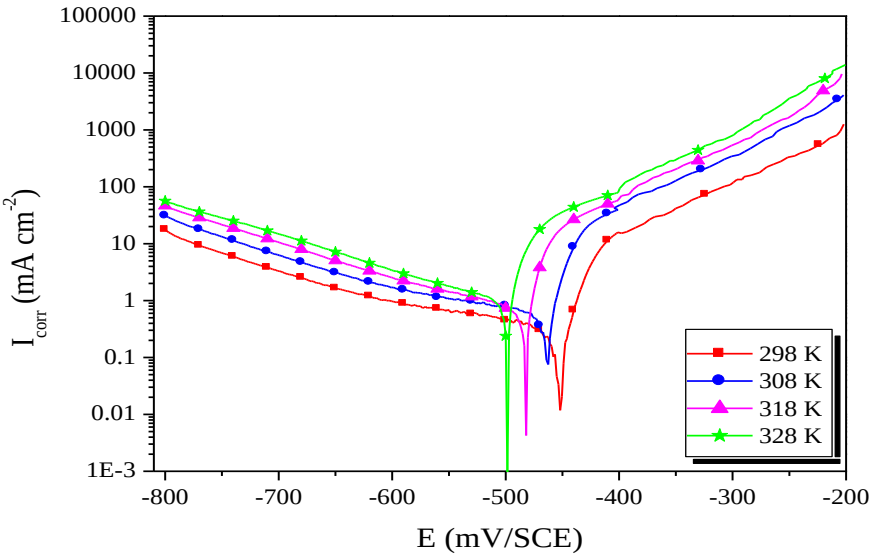

Figure 7. Potentiodynamic polarisation curves of carbon steel in 2.0 M H_3PO_4 in the presence of 10^{-3} M of PIP inhibitor at different temperatures.

Table 4. Various corrosion parameters for carbon steel in 2.0 M H_3PO_4 in absence and presence of optimum concentration of PIP at different temperatures.

Inhibitor	Temp (K)	E_{corr} (mV/SCE)	I_{corr} ($\mu A/cm^2$)	$-b_c$ (mV/dec)	η_p (%)
Blank	298	-488	2718	135	----
	308	-532	4220	137	----
	318	-523	6610	132	----
	328	-514	11890	139	----
PIP	298	-452	241.0	154	91.1
	308	-450	342.0	151	91.9
	318	-480	563.0	149	91.5
	328	-501	1029	156	91.3

The effect of temperature on the corrosion inhibition with and without PIP is shown in Table 4. Fig. 6 and Fig. 7, show the Tafel plots of carbon steel in 2.0 M H_3PO_4 in absence and presence of 10^{-4} M PIP in temperature range 298-328K. It can be seen that the corrosion current density increases with temperature in the absence and presence of PIP, and the values of inhibition efficiency of PIP are nearly constant in the temperature range studied (Table 4). The corrosion current density for steel increases more rapidly with temperature in the absence of inhibitor (blank). This result confirms that PIP acts as an efficient inhibitor in the range of temperature studied. The PIP inhibitor efficiency is temperature-independent. Adsorption and desorption of inhibitor molecules continuously occur at the metal surface and an equilibrium exists between two processes at a particular temperature. With

increase of temperature, the equilibrium between adsorption and desorption process is shifted towards desorption until equilibrium is established again at a different value of equilibrium constant.

Activation energy can be obtained by Arrhenius equation as follows:

$$I_{corr} = k \exp\left(-\frac{E_a}{RT}\right) \qquad (8)$$

where E_a is the apparent activation corrosion energy, R is the universal gas constant and k is the Arrhenius pre-exponential constant. Taking the logarithm of the Arrhenius equation yields:

$$LnI_{corr} = \frac{-E_a}{RT} + Lnk \qquad (9)$$

Potentiodynamic polarization measurements were utilized to obtain the I_{corr} values of carbon steel in the absence and presence of 10^{-3} M of PIP at different temperatures of 298, 308, 318 and 328K. These values were plotted as shown in Fig. 8. The values of activation energy of corrosion were determined from the slope of Ln (I_{corr}) versus 1/T plots [43]. The E_a values for carbon steel in the absence and presence of 10^{-3} M of PIP were calculated and listed in Table 5. It is clearly seen from the results obtained that the reduction of the activation energy in the presence of PIP may be attributed to the chemisorption of the PIP inhibitor on carbon steel surface. A transition state complex is decays to products after forming the high energy [44]. The mathematical form of transition state theory is shown as below:

$$I_{corr} = \frac{RT}{Nh} \exp\left(\frac{\Delta S_a}{R}\right) \exp\left(-\frac{\Delta H_a}{RT}\right) \qquad (10)$$

where I_{corr} is the corrosion rate, A is the pre-exponential factor, h is Planck's constant, N is the Avogadro number, R is the universal gas constant, ΔH_a is the enthalpy of activation and ΔS_a is the entropy of activation.

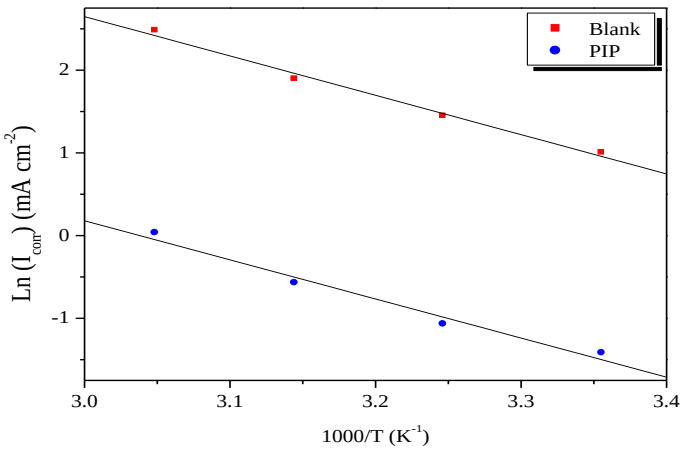

Figure 8. Arrhenius plots of carbon steel in 2.0 M H_3PO_4 with and without 10^{-3} M of PIP.

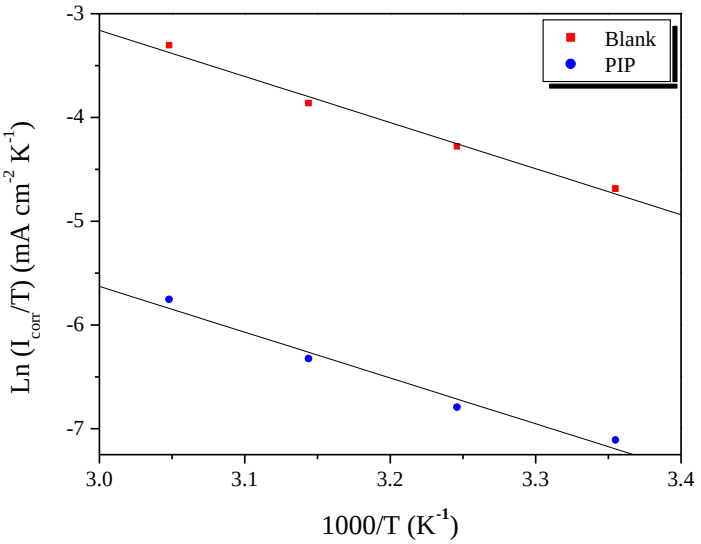

Figure 9. Relation between Ln (I_{corr}/ T) and 1000/T at different temperatures.

The values of enthalpy and entropy of activation for carbon steel corrosion in 2.0 M H_3PO_4 in absence and presence of PIP can be evaluated from the slope and intercept of the curve of Ln (I_{corr}/T) versus 1/T, respectively as shown in Fig. 9.

The values of enthalpy and entropy of activation for carbon steel corrosion are tabulated in Table 5. The positive signs of the enthalpies ΔH_a reflect the endothermic nature of the steel dissolution process and mean that the dissolution of carbon steel is difficult [45]. We remark that E_a and ΔH_a values vary in the same way (Table 5). This result permit to verify the known thermodynamic reaction between the E_a and ΔH_a as shown in Table 5 [46]:

$$\Delta H_a = E_a - RT \qquad (11)$$

The large negative values of entropies ΔS_a from PIP imply that the activated complex in the rate determining step represents an association rather than a dissociation step, meaning that a decrease in disordering takes place on going from reactants to the activated complex [47,48].

Table 5. The value of activation parameters E_a, ΔH_a and ΔS_a for carbon steel in 2.0 M H_3PO_4 in the absence and presence of 10^{-3} M of PIP.

Inhibitor	E_a (kJ/mol)	ΔH_a (kJ/mol)	ΔS_a (J/mol)	E_a -ΔH_a (KJ/mol)
Blank	39.50	36.91	-112.98	2.59
PIP	39.26	36.67	-134.20	2.59

3.3. Adsorption and thermodynamic considerations

The primary step in the action of inhibitors in acid solution is generally agreed to be adsorption on the metal surface. This involves the assumption that the corrosion reactions are prevented from occurring over the area (or active sites) of the metal surface covered by adsorbed inhibitor species, whereas these corrosion reaction occurred normally on the inhibitor free area [49]. Accordingly, the fraction of surface covered with inhibitor species calculated by equation (6) can followed as a function of inhibitor concentration and solution temperature. The surface coverage (θ) data are very useful while discussing the adsorption characteristics. When the fraction of surface covered is determined as a function of the concentration at constant temperature, adsorption isotherm could be evaluated at equilibrium condition. The dependence of the fraction of the surface covered θ on the concentration C of the inhibitor was tested graphically by fitting it to Langmuir's isotherm, which assumes that the solid surface contains a fixed number of adsorption sites and each site holds one adsorbed species. Fig. 10 shows the linear plots for C/ θ versus C with R^2 = 0.9999 correlation coefficient, suggestion that the adsorption obeys the Langmuir's isotherm:

$$\frac{C}{\theta} = \frac{1}{K} + C \qquad (12)$$

where C is the equilibrium inhibitor concentration, K adsorptive equilibrium constant, representing the degree of adsorption i.e., the higher the value of K indicates that the inhibitor is strongly adsorbed on the metal surface. The thermodynamics parameters derived from Langmuir adsorption isotherm for the studied compound, are given in Table 6.

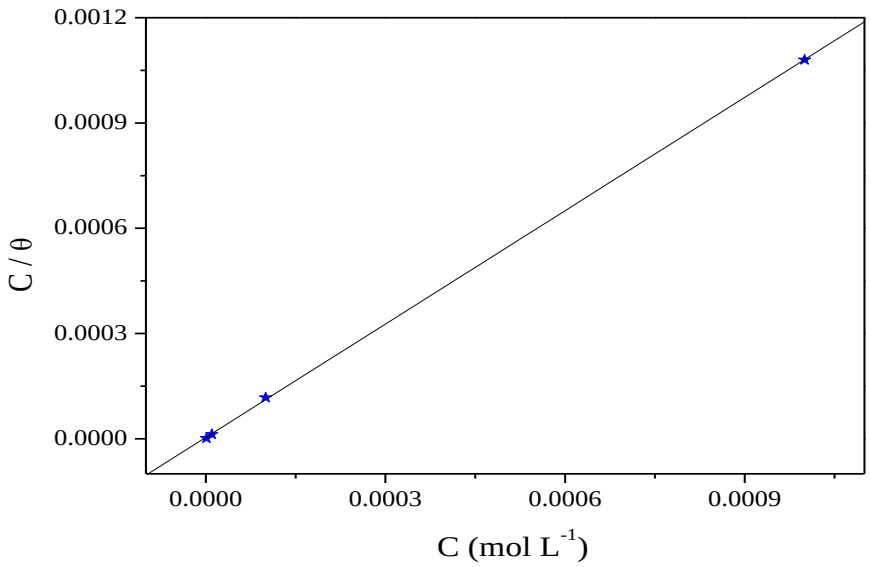

Figure 10. Langmuir adsorption of PIP on the carbon steel surface in 2.0 M H_3PO_4 solution.

The standard adsorption free energy ΔG°_{ads} was calculated using the following equation [50]:

$$\Delta G^{\circ}_{ads} = -RTLn(55.5K_{ads}) \quad (13)$$

Where R is gas constant and T is absolute temperature of experiment and the constant value of 55.5 is the concentration of water in solution in mol L^{-1}.

Table 6. Thermodynamic parameters for the adsorption of PIP in 2.0 M H_3PO_4 on the carbon steel at 298K.

Inhibitor	Slope	R_L	$K_{Langmuir}$ (M^{-1})	R^2	$K_{Kinetic}$ (M^{-1})	y	ΔG°_{ads} (kJ/mol)
PIP	1.05	0.00438	227270.14	0.9999	216162.12	0.35044	-40.51

The negative value of ΔG°_{ads} ensure the spontaneity of the adsorption process and stability of the adsorbed layer on the metal surface. Generally, value ΔG°_{ads} up to -20 kJ mol^{-1} is consistent with electrostatic interaction between the charged molecules and the charged metal (physisorption) while those around -40 kJ mol^{-1} or higher are associated with chemisorptions as a result of sharing or transfer of electrons from the molecules to the metal surface to form a coordinate type of bond [50]. While other researchers suggested that the range of ΔG°_{ads} of chemical adsorption processes for inhibitor in aqueous media lies between -21 and -42 kJ mol^{-1} [51]. Therefore, for present work the value of ΔG°_{ads} has been considered of chemisorption. Moreover, the essential characteristic Langmuir isotherm can be expressed in term of a dimensionless separation factor, R_L [51], which describe the type of isotherm and defined by:

$$R_L = \frac{1}{1+KC} \quad (14)$$

The smaller R_L value indicates a highly favorable adsorption. If $R_L > 1$ unfavorable, $R_L = 1$ linear,

$0 < R_L < 1$ favorable, and if $R_L = 0$ irreversible. Table 6 gives the estimated value of R_L for PIP at different 10^{-3} M. It was found that the R_L value is less than unity conforming that the adsorption processes is favorable.

Recent researches have looked into the action of an adsorptive inhibitor from a purely mechanistic kinetic point of view [51]. This relation can be expressed as follow:

$$\frac{\theta}{1-\theta} = K'C^{y} \quad (15)$$

or this equation can be writing in linear form as;

$$Ln\left(\frac{\theta}{1-\theta}\right) = LnK' + yLnC \quad (16)$$

where K' is a constant, and y is the number of inhibitor molecules occupying one active site. A plot of Ln (θ/1-θ) versus Ln (C) gives a straight line of slop y and intercept of Ln (K'), as shown in Fig. 11. Equilibrium constant corresponding to adsorption isotherm is given by, $K = K'^{1/y}$. Value of $y > 1$ implies the formation of multilayer of inhibitor on the surface of metal. Value of $y < 1$ mean a given inhibitor molecules will occupy more than one active site. The behavior of equilibrium constants obtained from Langmuir model was similar to the values which obtained by kinetic-thermodynamic model. Also the value of y was lower than unity indicating the formation of monolayer on the metal surface which agrees the assumptions of Langmuir adsorption isotherm.

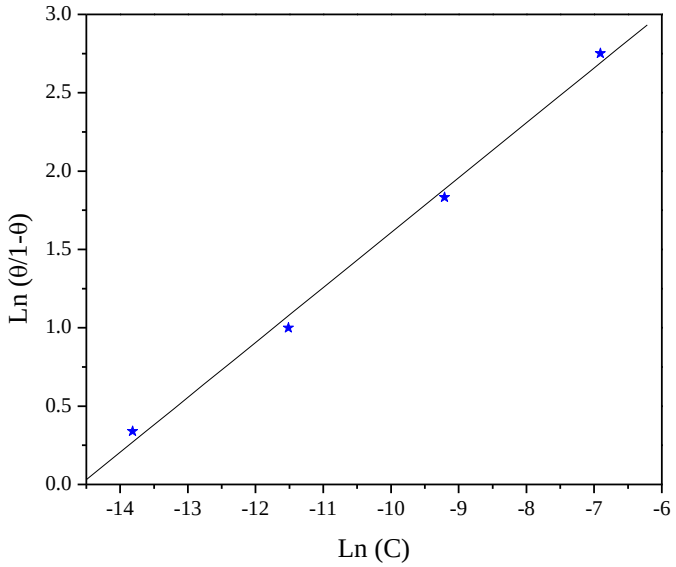

Figure 11. Kinetic–thermodynamic model for the adsorption of PIP on carbon steel surface.

3.4. Quantum chemical calculations

Quantum chemical calculations are utilized to ascertain whether there is a clear relationship between the molecular structures of the synthesized inhibitor and its inhibition effect. The structure parameters and adsorptive performance of the synthesized inhibitor are used to elucidate the inhibition mechanism in the present work. The equilibrium geometry structures and the frontier molecule orbital density distributions of the molecule are shown in Fig. 12, and the quantum chemical parameters are listed in Table 7.

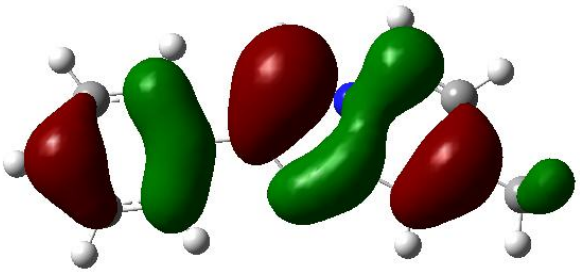

HOMO

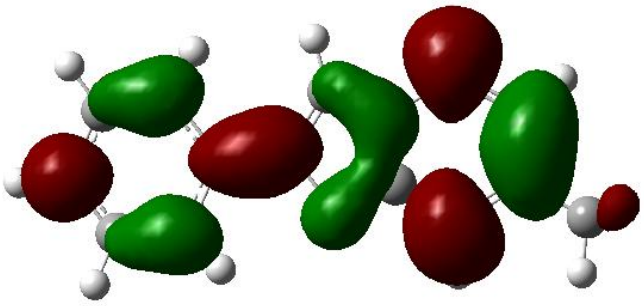

LUMO

Figure 12. Frontier molecule orbital density distributions of the synthesized inhibitor.

Analysis of Fig. 12 shows that the distribution of two energies HOMO and LUMO, we can see that the electron density of the HOMO and LUMO location was distributed almost of the entire molecule.

E_{HOMO} is often associated with the capacity of a molecule to donate electron. High value of E_{HOMO} probably indicates a tendency of the molecule to donate electrons to appropriate acceptor molecules with low energy and empty molecular orbital. E_{LUMO} indicates the ability of the molecule to accept electrons. The lower the value of E_{LUMO}, the more probable is that the molecule would accept electrons [52]. According to frontier orbital theory, the reaction of reactants mainly occurs on HOMO and LUMO [53]. So, the smaller gap (ΔE) between E_{HOMO} and E_{LUMO} is the more probable to donate and accept electrons. The values of ΔE in Table 7, suggesting the strongest ability of the synthesized inhibitor to form coordinate bonds with d-orbitals of metal through donating and accepting electrons, is in good agreement with the experimental results. Additionally, for the dipole moment (μ), higher value of μ will favor the enhancement of corrosion inhibition [54]. From Table 7, the value of μ is higher, which is also in agreement with the experimental results mentioned above.

Another method to correlate inhibition efficiency with parameters of molecular structure is to calculate the fraction of electrons transferred from inhibitor to metal surface. According to Koopman's theorem [55], E_{HOMO} and E_{LUMO} of the inhibitor molecule are related to the ionization potential (I) and the electron affinity (A), respectively. The ionization potential (I) and the electron affinity (A) are defined as follows:

$$I = -E_{HOMO} \quad (17)$$

$$A = -E_{LUMO} \quad (18)$$

The obtained values of I and A were considered for the calculation [56] of the electronegativity χ and the global hardness η in each of the tested molecule using the following relations:

$$\chi = \frac{I + A}{2} \quad (19)$$

$$\eta = \frac{I - A}{2} \quad (20)$$

During the interaction of the inhibitor molecule with bulk metal, electrons flow from the lower electronegativity molecule to the higher electronegativity metal until the chemical potential becomes equalized. The fraction of the transferred electron, ΔN, was estimated according to Pearson [56]

$$\Delta N = \frac{\chi_{Fe} - \chi_{inh}}{2(\eta_{Fe} + \eta_{inh})} \quad (21)$$

where a theoretical value for the electronegativity of bulk iron was used, χ (Fe) = 7 eV, and a global hardness of η (Fe) = 0 was used [57]. The calculated results are presented in Table 7. Generally, value of ΔN shows inhibition efficiency resulting from electron donation, and the inhibition efficiency increases with the increase in electron-donating ability to the metal surface. Value of ΔN show inhibition effect resulted from electrons donation. According to Lukovits's study [58], if ΔN < 3.6, the inhibition efficiency increases with increasing electron-donating ability at the metal surface. Based on these calculations, it is expected that the synthesized inhibitor is donor of electrons, and the steel surface is the acceptor, and this favors chemical adsorption of the inhibitor on the electrode surface. Here the inhibitor binds to the steel surface and forms an adsorption layer against corrosion. The synthesized inhibitor shows the highest inhibition efficiency because it has the highest HOMO energy and this reflects the greatest ability (the lowest ΔE) of offering electrons. It can be seen from Table 7 that the ability of the synthesized inhibitor to donate electrons to the metal surface, which is in good agreement with the higher inhibition efficiency of the synthesized inhibitor.

Table 7. Calculated quantum chemical parameters of the studied compound.

Quantum parameters	PIP
E_{HOMO} (eV)	-5.4489
E_{LUMO} (eV)	-0.9470
ΔE gap (eV)	4.5018
μ (debye)	3.4302
$I = -E_{HOMO}$ (eV)	5.4489
$A = -E_{LUMO}$ (eV)	0.9470
$\chi = \frac{I + A}{2}$ (eV)	3.19795
$\eta = \frac{I - A}{2}$ (eV)	2.25095
$\Delta N = \frac{\chi_{Fe} - \chi_{inh}}{2(\eta_{Fe} + \eta_{inh})}$	0.8445434
TE (eV)	-17686.29

4. SUMMARY

The compound 7-methyl-2-phenylimidazo[1,2-α]pyridine (PIP) is a good corrosion inhibitor at low concentrations. Inhibition efficiency increases with increase in PIP concentration, but decrease with increase in temperature. Potentiodynamic polarization results revealed that PIP in 2.0 M H_3PO_4 solution acted as a mixed-type inhibitor, which decreases the cathodic, anodic, and corrosion currents to a great extent. EIS measurement results indicate that the resistance of the carbon steel electrode increases greatly and its capacitance decreases by increasing the inhibitor concentration. Adsorption of inhibitor obeys Langmuir adsorption isotherm by forming a monolayer on metal surface. Through the quantum chemical calculations, it was shown that calculated parameters were correlated with the experimental results.

ACKNOWLEDGEMENTS
Prof S. S. Al-Deyab and Prof B. Hammouti extend their appreciation to the Deanship of Scientific Research at king Saud University for funding the work through the research group project.

References

1. L. Larabi, O. Benali, Y. Harek, *Mater. Let*. 61 (2007) 3287.
2. Y. Abboud, A. Abourriche, T. Saffaj, M. Berrada, M. Charrouf, A. Bennamara, A. Cherqaoui, D. Takky, *Appl. surf. Sci*. 252 (2006) 8178.
3. Belkhaouda, M., Bazzi, L., Salghi, R., Benlhachemi, A., Hammouti, B., El Issami, S., Hilali, M., *Phys. chem. News*. 45 (2009) 137.
4. A. El Bribri, M. Tabyaoui, B. Tabyaoui, H. El Attari, F. Bentis, *Materials Chemistry and Physics*, 141 (2013) 240.
5. F. Bentiss, M. Traisnel, L. Gengembre, M. Lagrenée, *Appl. Surf. Sci*, 152 (1999) 237.
6. H. Zarrok, A. Zarrouk, R. Salghi, H. Oudda, B. Hammouti, M. Assouag, M. Taleb, M. Ebn Touhami, M. Bouachrine and S. Boukhris, *J. Chem. Pharm. Res*. 4 (2012) 5056.
7. H. Zarrok, A. Zarrouk, R. Salghi, Y. Ramli, B. Hammouti, M. Assouag, E. M. Essassi, H. Oudda and M. Taleb, *J. Chem. Pharm. Res*. 4 (2012) 5048.
8. Y. Elkacimi, M. Achnin, Y. Aouine, M.E. Touhami, A. Alami, R. Touir, M. Sfaira, D. Chebabe, A. Elachqar, B. Hammouti, *Portug. Electrochim. Acta*, 30 (2012) 53.
9. L. Wang, *Corros. Sci*, 43 (2001) 2281.
10. A. Popova, M. Christov, T. Deligeorgiev, *Corrosion*, 59 (2003) 756.
11. A. Zarrouk, M. Messali, M. R. Aouad, M. Assouag, H. Zarrok, R. Salghi, B. Hammouti, A. Chetouani, *J. Chem. Pharm. Res*. 4 (2012) 3427.
12. M. Elbakri, R. Touir, M. Ebn Touhami, A. Zarrouk, Y. Aouine, M. Sfaira, M. Bouachrine, A. Alami, A. El Hallaoui, *Res. Chem. Intermed*. (2012) DOI: 10.1007/s11164-012-0768-6.
13. K. F. Khaled, *Electrochim. Acta*, 48 (2003) 2493.
14. H. Bendaha, A. Zarrouk, A. Aouniti, B. Hammouti, S. El Kadiri, R. Salghi, R. Touzani, *Phys. Chem. News*, 64 (2012) 95.
15. F. Zhang, Y. Tang, Z. Cao, W. Jing, Z. Wu, Y. Chen, *Corros. Sci*, 61 (2012) 1.
16. A. Ghazoui, R. Saddik, B. Hammouti, A. Zarrouk, N. Benchat, M. Guenbour, S. S. Al-Deyab, I. Warad, *Res. Chem. Intermed*. (2012) DOI: 10.1007/s11164-012-0763-y.
17. I. B. Obot, N.O. Obi-Egbedi, *Corros. Sci*, 52 (2010) 657.

18. I. Ahamad, M.A. Quraishi, *Corros. Sci*, 51 (2009) 2006.
19. D. Ben Hmamou, R. Salghi, A. Zarrouk, M. Messali, H. Zarrok, M. Errami, B. Hammouti, Lh. Bazzi , A. Chakir, *Der Pharm. Chem*. 4 (2012) 1496.
20. I. Ahamad, M.A. Quraishi, *Corros. Sci*, 52 (2010) 651.
21. A. Popova, M. Christov, A. Vasilev, *Corros. Sci*, 49 (2007) 3290.
22. Y. Abed, B. Hammouti, M. Taleb, S. Kertit, *Transactions of the SAEST*, 37 (2002) 99.
23. H. Zarrok, H. Oudda, A. El Midaoui, A. Zarrouk, B. Hammouti, M. Ebn Touhami, A. Attayibat, S. Radi, R. Touzani, *Res. Chem. Intermed*. (2012) DOI: 10.1007/s11164-012-0525-x.
24. H. Zarrok, R. Salghi, A. Zarrouk, B. Hammouti, H. Oudda, Lh. Bazzi, L. Bammou, S. S. Al-Deyab, *Der Pharm. Chem*. 4 (2012) 407.
25. A. Ghazoui, R. Saddik, N. Benchat, B. Hammouti, M. Guenbour, A. Zarrouk, M. Ramdani, *Der Pharm. Chem*. 4 (2012) 352.
26. H. Zarrok, R. Saddik, H. Oudda, B. Hammouti, A. El Midaoui, A. Zarrouk, N. Benchat, M. Ebn Touhami, *Der Pharm. Chem*. 3 (2011) 272.
27. H. Zarrok, A. Zarrouk, B. Hammouti, R. Salghi, C. Jama, F. Bentiss, *Corros. Sci*. 64 (2012) 243.
28. R. Salghi, A. Zarrouk, H. Zarrok, M. Assouag, B. Hammouti, S. S. Al-Deyab, M. El Hezzat, Der Pharmacia Lettre, 5 (2) (2013) 135
29. N.J. Walton, M.J. Mayer, A. Narbad, *Phytochemistry*, 63 (2003) 505.
30. A.Y. El-Etre, *Corros. Sci*. 43 (2001) 1031.
31. K.C. Emregül, M. Hayvalı, *Mater. Chem. Phys*. 83 (2004) 209.
32. A.D. Becke, *J. Chem. Phys*. 96 (1992) 9489.
33. A.D. Becke, *J. Chem. Phys*. 98 (1993) 1372.
34. C. Lee, W. Yang, R.G. Parr, *Phys. Rev. B*. 37 (1988) 785.
35. Gaussian 03, Revision B.01, M. J. Frisch, et al., Gaussian, Inc., Pittsburgh, PA, (2003).
36. Y. Yan, W. Li, L. Cai, B. Hou, *Electrochim. Acta*. 53 (2008) 5953.
37. N. Labjar, M. Lebrini, F. Bentiss, N.E. Chihib, S. El Hajjaji, C. Jama, *Mater. Chem. Phys*. 119 (2010) 330.
38. M. Lebrini, M. Lagrenee, H. Vezin, M. Traisnel, F. Bentiss, *Corros. Sci*. 49 (2007) 2254.
39. K.F. Khaled, N. Hackerman, *Mater. Chem. Phys*. 82 (2003) 949.
40. M. Christov, A. Popova, *Corros. Sci*, 46 (2004) 1613.
41. M. Scendo, *Corros. Sci*. 50 (2008) 1584.
42. K.F. Khaled, *Mater. Chem. Phys*. 125 (2011) 427.
43. R. Sanchez-Tovar, M.T. Montanes, J. Garcia-Anton, *Corros. Sci*. 52 (2010) 722.
44. A.A. Khadom, A.S. Yaro, A.A.H. Kadhum, A.S. Al Taie, A.Y. Musa, *Amer. J. Appl. Sci*. 6 (2009) 1403.
45. B. Hammouti, A. Zarrouk, S.S. Al-Deyab And I. Warad, *Orient. J. Chem.,* 27 (2011) 23.
46. F. Bentiss, M. Traisnel, H. Vezin, M. Lagrenée, *Corros. Sci, 45 (2003)371*.
47. S. Martinez, I. Stern, *Appl. Surf. Sci*. 199 (2002) 83.
48. S. L. Granese, B.M. Rosales, C. Oviedo, J.O. Zerbino, *Corros. Sci*. 33 (1992) 1439.
49. L.L. Shereir, Corrosion, vol. 2, second ed., Newnes-Butterworths, London, 1977.
50. S.A. Umoren, E.E. Ebenso, *Mater. Chem. Phys*. 106 (2007) 393.
51. A.A. Khadom, A.S. Yaro, A.S. AlTaie, A.A.H. Kadum, *Portug. Electrochim. Acta* 27 (6) (2009) 699.
52. M.M. Ibrahim, M.A. Amin, K. Ichikawa , *J. Mol. Struct*. 985 (2011) 191.
53. N. Khalil, *Electrochim. Acta* 48 (2003) 2635.
54. J. Zhang, J. Liu, W. Yu, Y. Yan, L. You, L. Liu, *Corros. Sci*. 52 (2010) 2059.
55. M. Lebrini, M. Lagrenee, M. Traisnel, L. Gengembre, H. Vezin, F. Bentiss, *Appl. Surf. Sci*. 253 (2007) 9267.
56. G. Pearson, *Inorg. Chem*. 27 (1988**)** 734.
57. T. Arslan, F. Kandemirli, E.E. Ebenso, I. Love and H. Alemu, *Corros. Sci*., 51 (2009) 35.

58. I. Lukovits, E. Kalman, F. Zucchi, *Corrosion* 57 (2001) 3.

© 2013 by ESG (www.electrochemsci.org)